sustainable chemistry

MDPI

Article

Transformation of Ibuprofen- and Diclofenac-Loaded Organobentonites to Doped Carbons for Peroxide Production and Energy Storage

Milena Obradović [1], Maja Ranković [2], Anka Jevremović [2], Aleksandra Daković [1], Bojana Nedić Vasiljević [2], Danica Bajuk-Bogdanović [2], Hong Wang [3], Maja Milojević-Rakić [2] and Nemanja Gavrilov [2,*]

[1] Institute for Technology of Nuclear and Other Mineral Raw Materials, Franše d' Eperea 86, 11000 Belgrade, Serbia; m.obradovic@itnms.ac.rs (M.O.); a.dakovic@itnms.ac.rs (A.D.)
[2] Faculty of Physical Chemistry, University of Belgrade, Studentski Trg 12–16, 11158 Belgrade, Serbia; maja.rankovic@ffh.bg.ac.rs (M.R.); anka@ffh.bg.ac.rs (A.J.); bojana@ffh.bg.ac.rs (B.N.V.); danabb@ffh.bg.ac.rs (D.B.-B.); maja@ffh.bg.ac.rs (M.M.-R.)
[3] School of Chemical Engineering & Technology, China University of Mining and Technology, Xuzhou 221116, China; hongwang@cumt.edu.cn
* Correspondence: gavrilov@ffh.bg.ac.rs

Abstract

Ibuprofen- and diclofenac-loaded organobentonites are thermally converted to carbon-decorated bentonites and probed as materials for supercapacitors and peroxide production. TGA shows a ~40% mass loss in an inert atmosphere and a ~2% further reduction in air, with the diclofenac-loaded sample showing slightly higher loss due to less stable surface groups. FTIR and Raman spectroscopies indicate similar surface groups and defect densities in the end materials, which are reflected in similar electrochemical responses. Capacitance values of around 20 F/g are measured when taking the whole mass, bentonite and carbon, into account, rising to a maximum of 805 F/g if only the carbon fraction is taken into account. Rotating ring–disk measurements reveal that the prepared materials show selectivity toward peroxide production when oxygen reduction is probed, reaching a 93% yield, making it an exceptional candidate for peroxide production.

Keywords: peroxide production; adsorbent repurposing; carbon materials; capacitance; carbonization

1. Introduction

The increasing occurrence of pharmaceutical contaminants in aquatic environments has become a significant environmental concern due to their persistence, incomplete removal in conventional wastewater treatment plants, and potential adverse effects on aquatic organisms and the ecosystem [1–4]. Non-steroidal anti-inflammatory drugs (NSAIDs) are among the most frequently detected pharmaceutical compounds in surface waters, groundwater, and wastewater effluents because of their widespread consumption and extensive use in human medicine [5–8]. Their continuous discharge into the environment highlights the need for cost-effective and sustainable treatment technologies that can efficiently remove these contaminants while enabling the valorization of the resulting waste materials [9]. Adsorption is widely considered one of the most practical approaches for the removal of pharmaceutical compounds because of its simplicity and compatibility with a broad range of adsorbent materials [10,11]. Bentonite has attracted considerable attention as an

Check for updates

Academic Editor: Raffaele Cucciniello

Received: 10 July 2026
Revised: 25 August 2026
Accepted: 1 September 2026
Published: 4 September 2026

Copyright: © 2026 by the authors. Licensee MDPI, Basel, Switzerland. This article is an open access article distributed under the terms and conditions of the Creative Commons Attribution (CC BY) license.

adsorbent owing to its abundance, low cost, layered structure, high cation-exchange capacity (CEC), and tunable surface properties. However, pristine bentonite generally exhibits limited affinity toward many organic contaminants due to its intrinsically hydrophilic nature and negatively charged surface [12,13].

Surface modification using surfactants has emerged as an effective strategy for improving the adsorption properties of bentonite [14–16]. Cationic surfactants such as hexadecyltrimethylammonium bromide (HDTMA-Br), tetradecyltrimethylammonium bromide (TDTMA-Br), and octadecylammonium bromide (ODA-Br), as well as related quaternary ammonium compounds, can intercalate within bentonite layers and at the surface, altering the surface chemistry from hydrophilic to organophilic [17]. This modification can increase interlayer space and generate hydrophobic domains that facilitate interactions with organic contaminants through hydrophobic interactions, partitioning effects, and electrostatic attraction. Previous studies have demonstrated substantially enhanced adsorption capacities of surfactant-modified bentonite for dyes, humic substances, bisphenol compounds, and pharmaceutical pollutants [16,18,19]. Surfactant-modified bentonites have been widely explored as adsorbents for the removal of pharmaceutical contaminants, including antibiotics, NSAIDs, endocrine-disrupting compounds, and other emerging organic pollutants from aqueous media. The enhanced adsorption was frequently associated with electrostatic interactions and hydrophobic partitioning effects introduced by surfactant molecules [20]. For example, in our previous studies, bentonites modified with various amounts (50, 75, and 100% of CEC) of octadecyldimethylbenzylammonium chloride (ODMBA-Cl) and HDTMA-Br were tested as adsorbents for ibuprofen (IBU) and diclofenac sodium (DS) [21–23]. The adsorption of both drugs increased with increasing amounts of both surfactants as well as with increasing the initial concentrations of IBU and DS. The maximum adsorbed amounts of the drugs were 102 mg/g for IBU and 160 mg/g for DS on organobentonite containing 100% ODMBA, while for organobentonite modified with 100% HDTMA, the maximum adsorbed amounts were 89 mg/g and 150 mg/g for IBU and DS, respectively [23]. These drug adsorption capacities were close to the highest values reported in the literature for organobentonites with similar amounts of surfactants [24–26]. Characterization of the organobentonites with the highest amounts of both surfactants after IBU and DS adsorption confirmed the presence of drugs in the organobentonites [23].

Despite considerable progress in improving adsorption performance, one of the principal limitations of adsorption technologies remains the management of exhausted adsorbents after contaminant uptake [27,28]. Spent adsorbents are often regarded as secondary waste requiring disposal or regeneration, increasing process costs and reducing overall sustainability. Recent research has therefore shifted toward circular-material concepts in which exhausted adsorbents are transformed into functional materials with additional applications [29–31]. Carbonization processes conducted under inert atmospheres represent a promising route since organic compounds adsorbed on the adsorbent surface can serve as carbon precursors for the generation of conductive carbon structures [32]. Carbon-containing bentonite-based materials have shown favorable structural characteristics, such as hierarchical porosity, high surface area, and enhanced electrical conductivity, making them suitable candidates for electrochemical applications. Carbon-based hybrid materials have become particularly attractive for electrochemical energy storage and electrocatalysis due to their tunable surface chemistry and structural versatility [32–34]. In supercapacitor applications, conductive carbon networks combined with porous support materials can improve charge transfer and increase electrolyte accessibility, resulting in enhanced specific capacitance and cycling stability [35–37]. Likewise, heteroatom-containing carbon materials have shown significant potential as catalysts for the oxygen reduction reaction (ORR), an electrochemical process of central importance for fuel cells and metal–air batteries.

The presence of defects, surface functionalities, and heteroatom species generated during carbonization can create catalytically active sites and improve ORR kinetics [38].

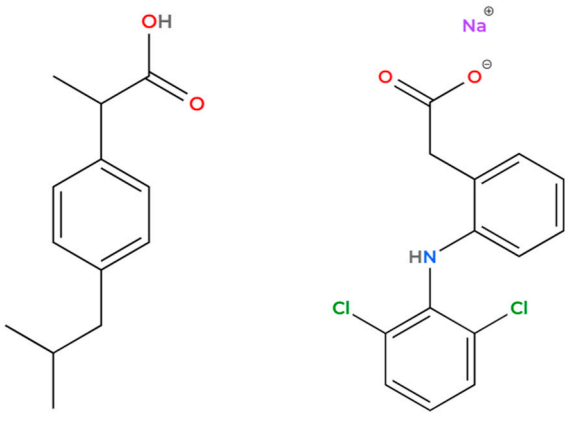
Beyond adsorption, the transformation of organobentonites into functional carbon-based materials via thermal treatment offers an attractive pathway for valorization and multifunctional applications [39]. Carbonization of surfactant-modified clays under inert atmospheres yields hybrid carbon–inorganic composites, in which the organic modifier serves as a carbon precursor [40–42]. Such materials can exhibit enhanced electrical conductivity, hierarchical porosity, and heteroatom doping, making them promising candidates for electrochemical applications, including ORR catalysis and energy storage in supercapacitors.

In this context, previously studied surfactant-modified bentonites with 100% CEC of HDTMA and ODMBA saturated with IBU and DS [23] are further explored here in terms of the carbonization process, and the resulting materials are evaluated as multifunctional systems. By linking the initial adsorption performance to the properties of the derived carbonized composites, this work aims to establish a relationship that bridges environmental remediation and energy-related applications. Particular emphasis is placed on understanding how the adsorbed drugs influence the physicochemical characteristics of the carbonized materials and their performance in electrochemical systems. Unlike conventional methods requiring additional carbon precursors, this strategy utilizes the adsorbed contaminants themselves as carbon sources, transforming a waste stream into a functional material. The resulting hybrid carbon–bentonite material was investigated as an electrode material for supercapacitor applications and as an electrocatalyst for the oxygen reduction reaction.

2. Materials and Methods

2.1. Sample Preparation

Bentonite, a natural mineral raw material from the Šipovo deposit (Bosnia and Herzegovina), was modified with two surfactants at loadings equal to 100% of its cation-exchange capacity. The surfactants used were HDTMA-Br (Sigma-Aldrich, St. Louis, MO, USA) and ODMBA-Cl (Hoechst AG, Frankfurt, Germany), following a previously reported procedure [22]. The organobentonites obtained with HDTMA and ODMBA are denoted as HB and OB, in that order. Ibuprofen (IBU; Galenika, LLC, Belgrade, Serbia) and diclofenac sodium (DS; Sigma-Aldrich, St. Louis, MO, USA) were used as test adsorbents; Scheme 1.



(**a**) (**b**)

Scheme 1. (**a**) IBU and (**b**) DS structures.

Powdered samples of the saturated organobentonites were collected after the adsorption of the IBU and DS drugs at an initial concentration of 500 mg/L [23]. The adsorbents were separated and subsequently thermally treated in an Ar atmosphere for 2 h at 800 °C in

a tubular furnace (Elektron, Banja Koviljača, Serbia). The carbonized organobentonites are labeled as c-HB and c-OB. The carbons derived from NSAID-saturated organobentonites are denoted as c-IBU@OB, c-DS@OB, c-IBU@HB, and c-DS@HB.

2.2. Sample Characterization

The quantitative measurement of NSAID residues, after carbonization, on the OB and HB systems was examined through a thermogravimetric (TG) analysis using an SDT 2960 thermoanalytical device (TA Instruments, New Castle, DE, USA). The thermal properties were investigated as the temperature was increased from ambient conditions to 800 °C (2 h holding time), at a heating rate of 10 °C min^{-1}, in either an inert (Ar) atmosphere or a synthetic air stream flowing at 80 mL min^{-1}.

The surface morphology of the samples was investigated using a Phenom ProX scanning electron microscope (Thermo Fisher Scientific, Waltham, MA, USA). Micrographs were collected at a magnification of 10,000×, employing a backscattered electron detector (BSD Full, Thermo Fisher Scientific, Waltham, MA, USA) operated at an accelerating voltage of 15 kV in map mode.

The chemical structure of the composites was investigated by Fourier transform infrared (FTIR) spectroscopy using a Nicolet iS20 spectrometer (Thermo Scientific, Waltham, MA, USA). Spectra were obtained by the KBr pellet method in the 4000–400 cm^{-1} region with a resolution of 4 cm^{-1} and 32 co-added scans. Raman characterization was carried out using a DXR Raman microscope (Thermo Scientific, Waltham, MA, USA) equipped with a 532 nm excitation laser. Sample visualization and laser focusing were performed using an Olympus optical microscope (Thermo Scientific, Waltham, MA, USA)fitted with a 10× objective lens. The Raman signal was dispersed through a 900 lines mm^{-1} diffraction grating. The spectra were recorded at 10 mW after confirming that no evident changes occurred as the laser power increased continuously. The laser spot had an approximate diameter of 2.1 μm, while the acquisition time was 10 s per scan and there were 10 accumulations for each measurement. To ensure representative sampling, spectra were collected from ten randomly selected locations on each sample surface, and the final spectrum was obtained by averaging the individual measurements.

2.3. Electrochemistry

Electrochemical measurements were performed using a glassy carbon (GC) electrode modified with a thin film of each carbonized sample. The catalyst ink was prepared by dispersing 5 mg of the samples in 0.5 mL of an ethanol/water/Nafion mixture under ultrasonic treatment. A catalyst loading of 250 μg cm^{-2} was achieved by drop-casting 5 μL of the suspension onto a GC disk electrode (5 mm diameter) and allowing it to dry at room temperature.

The ORR activity was evaluated by cyclic voltammetry (CV) in a conventional three-electrode electrochemical cell. A platinum wire and a saturated calomel electrode (SCE) served as the counter and reference electrodes, respectively, while a 0.1 M KOH aqueous solution was used as the supporting electrolyte. All measurements were conducted using an Ivium VO1107 potentiostat/galvanostat (Ivium Technologies, Eindhoven, The Netherlands). Before and throughout the measurements, the electrolyte was continuously saturated with oxygen by a gentle oxygen flow. Baseline voltammograms were recorded after purging the solution with nitrogen to remove dissolved oxygen and suppress oxygen-dependent electrochemical processes. All the experiments were performed under ambient conditions at atmospheric pressure and room temperature.

ORR activity was also investigated using a rotating ring–disk electrode (RRDE, glassy carbon disk/Pt ring, Gamry Instruments, Warminster, PA, USA) in an oxygen-saturated

0.1 M KOH solution. The catalyst-coated glassy carbon disk served as the working electrode, while the platinum ring was employed for the detection of peroxide intermediates. RRDE measurements were performed at various rotation rates to evaluate the oxygen reduction kinetics, electron transfer pathways, and hydrogen peroxide yield. The HO_2^- yield was calculated using Equation (1):

$$\%HO_2^- = 2(I_{ring}/N)/(I_{disc} + I_{ring}/N) \quad (1)$$

where I_{ring} is the ring current, I_{disc} is the disk current, and N is the collection efficiency.

To assess the charge-storage properties of composite samples, electrochemical measurements were performed at room temperature in 3 M KOH, 1 M Na_2SO_4, and 1 M H_2SO_4 aqueous electrolytes under a continuous nitrogen atmosphere to eliminate dissolved oxygen. The capacitance (C, F g^{-1}) was determined from the voltammetry data using Equation (2):

$$C = Q/2\ m\Delta V = (\int idt)/2\ m\Delta V \quad (2)$$

where Q is the total charge obtained by integrating the current response over time, ΔV denotes the potential window, and m corresponds to the mass of the active material loaded onto the glassy carbon electrode. All values are reported as the mean of 5 independent measurements on the same material.

Two-electrode measurements were performed in a symmetric setup in a lab-made cell, with aluminum (1 cm diameter) current collectors. Potential was scanned between 0 and 0.9 V, and the capacitance of a single electrode, Cs, was calculated using Equation (3):

$$Cs = 2\ I \cdot t_D/m_e \cdot \Delta V \quad (3)$$

where I is the applied current (0.5, 1, 2 A g^{-1}), t_D is the discharging time, m_e is the mass of active material on a single electrode, and ΔV is the potential window of the discharging process.

3. Results and Discussion

3.1. SEM/EDX

The SEM micrographs (Figure 1) reveal that all the carbonized NSAID-loaded organobentonites retain the characteristic agglomerated morphology of bentonite [34] while developing a rough, porous surface as a result of carbonization. No significant morphological differences are observed between the samples, although c-IBU@HB exhibits a more compact surface, whereas c-DS@HB displays a more heterogeneous and porous texture. The EDX analysis confirms the predominance of oxygen and silicon originating from the clay matrix, with carbon contents ranging from 14.5 to 34.0 at. % depending on the surfactant and adsorbed drug. The highest carbon content was observed for c-IBU@OB, while nitrogen was detected in samples saturated with DS prior to carbonization. These compositional differences indicate that both the organobentonite modifiers and the adsorbed drug influence the composition of the carbonaceous phase, which is expected to affect the electrochemical properties of the resulting materials.

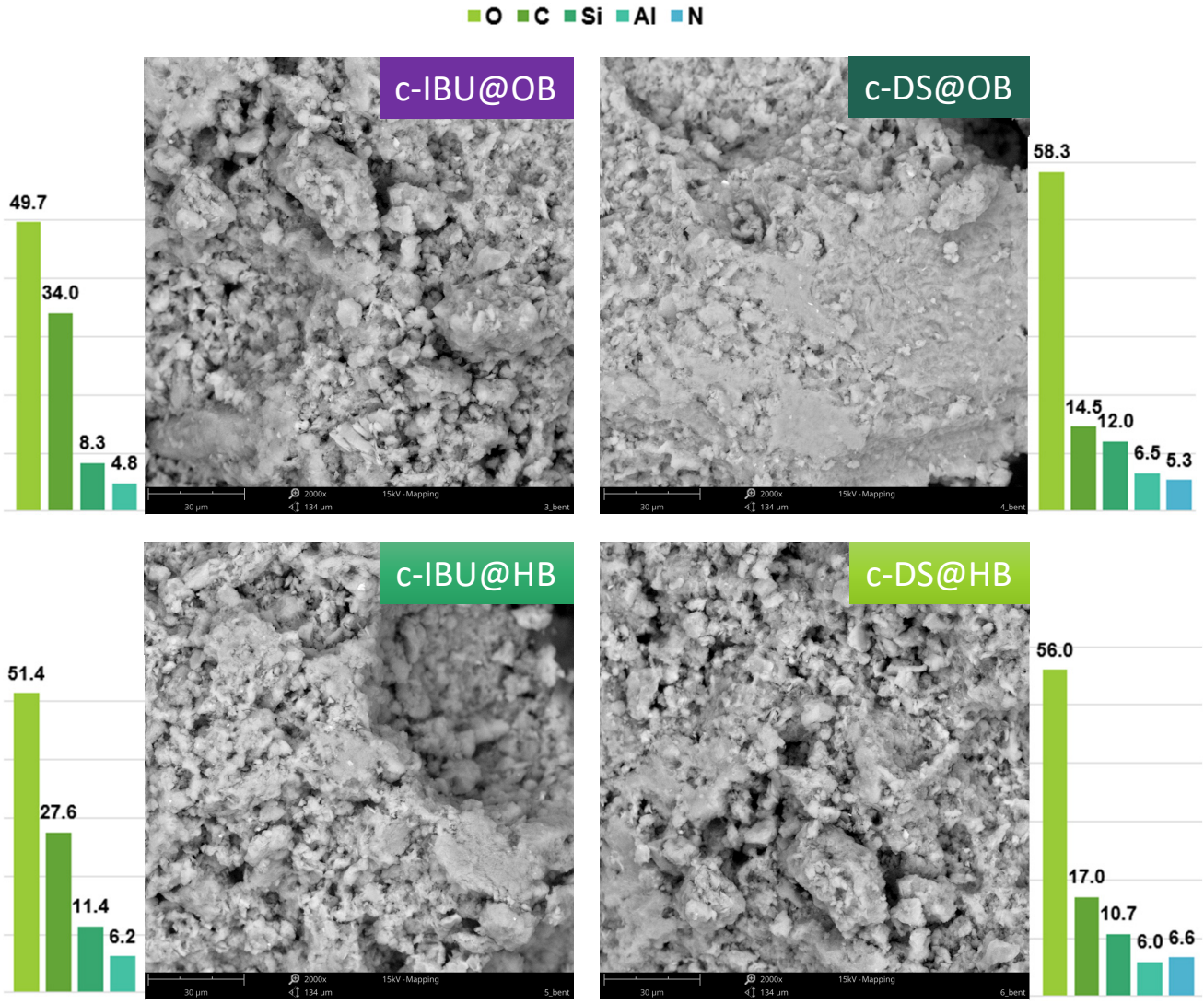
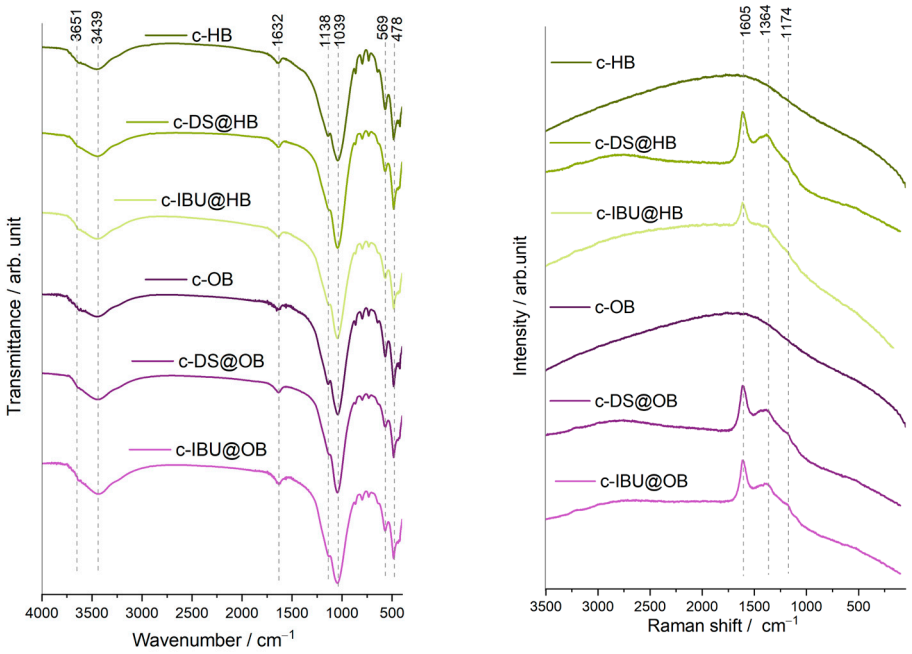


Figure 1. Surface morphology and elemental composition of carbonized HDTMA- and ODMBA-modified bentonites saturated with IBU and DS.

3.2. FTIR and Raman Spectroscopy

The FTIR spectra of the carbonized organobentonite samples and their drug-loaded counterparts are presented in Figure 2a. All the spectra exhibit similar profiles characteristic of the inorganic matrix (bentonite) [43]. A broad band centered at 3440 cm^{-1} was attributed to the stretching vibrations of hydroxyl groups associated with adsorbed water. The shoulder at 3651 cm^{-1} was assigned to the stretching vibrations of residual structural hydroxyl groups of the bentonite matrix. The weak absorption at 1632 cm^{-1} corresponded to the bending vibration of molecular water and may also include contributions from aromatic C=C vibrations within the carbonaceous phase. The most prominent feature in all the spectra was the intense band in the 1200–900 cm^{-1} region, centered at 1039 cm^{-1}, with a shoulder at approximately 1039 cm^{-1}, characteristic of Si–O elongation of the layered montmorillonite structure. Additional bands at 569 and 478 cm^{-1} were assigned to Si–O–Al and Si–O–Si deformation modes, confirming the preservation of the bentonite structure after carbonization [34].



(**a**) (**b**)

Figure 2. (**a**) FTIR and (**b**) Raman spectra of the HB- and OB-derived carbonized materials.

Comparison of the FTIR spectra of the HB- and OB-derived carbonized materials revealed no significant differences in the positions or relative intensities of the characteristic bands. These findings suggest that the type of surfactant has little influence on the chemical structure of the carbonized products, as the organic modifiers are largely decomposed during carbonization. Following adsorption of DS and IBU, no new bands or significant shifts were detected, indicating that adsorption proceeds primarily through non-covalent interactions, such as hydrophobic, electrostatic, and π–π interactions, rather than through the formation of new chemical bonds.

Generally, C–C stretching vibrations give rise to only weak IR absorption bands, whereas Raman spectroscopy is highly sensitive to symmetric homonuclear bonds. Consequently, the carbonaceous phase is more clearly resolved in the Raman spectra than in the FTIR spectra.

The Raman spectra of the samples are shown in Figure 2b. The Raman spectra of all the samples exhibited a pronounced fluorescence background. In the samples prior to drug adsorption, this fluorescence masks any Raman bands, whereas characteristic Raman features become observable in the drug-loaded carbonized organobentonite samples. These samples exhibited the characteristic Raman features of disordered carbonaceous structures, dominated by the G band at 1605 cm^{-1} and a broad D band centered at 1364 cm^{-1}. The D band is associated with structural defects, disorder, and edge sites within the carbon matrix, whereas the G band originates from the stretching vibrations of sp^2-hybridized carbon atoms in graphitic domains. The presence of both bands confirmed the formation of partially graphitized carbon during the carbonization process. Additionally, a band at approximately 1174 cm^{-1} was observed, which has been reported by Schwan et al. to correlate with the sp^3 bonding content in carbon films [44].

The Raman profiles of all the drug-loaded carbonized organobentonite samples are similar, indicating that neither the surfactant used for organobentonite preparation nor the adsorbed drug significantly alters the carbon framework. The positions and intensity ratios of the D and G bands remain unchanged, suggesting that the degree of graphitization and defect density are independent of both the surfactant used and the adsorbed drug.

3.3. Thermogravimetric Analysis

To assess the NSAID/surfactant conversion, we conducted the initial measurement in an inert atmosphere [45], where a TG analysis revealed 40% mass loss during the temperature treatment. The estimate of the amount of carbon residue on bentonite was performed using synthetic air as the carrier gas, with the mass loss attributed to carbon burn-off (Figure 3a). Contrary to expectations, the thermal behavior of the carbonized composites is governed predominantly by the nature of the adsorbed drug rather than by the type of surfactant initially used for organobentonite preparation [46].

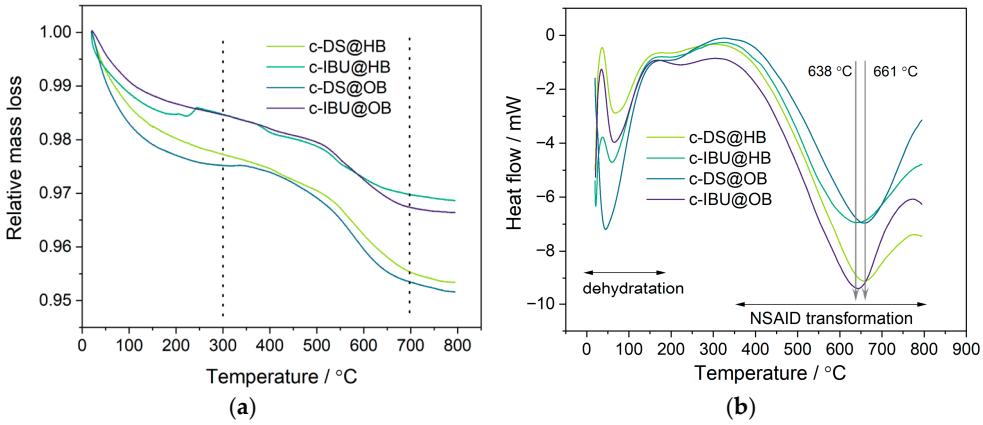


Figure 3. (**a**) TG and (**b**) DTA profiles of the HB- and OB-derived carbonized materials.

Up to 300 °C, water loss between 1.5 and 2.5 wt.% is evident, with samples initially loaded with DS losing around 1 wt.% more water than those loaded with IBU, indicating that more hydrophilic groups remained on the surface after carbonization (expected based on IBU and DS structures, Scheme 1).

Between 400 and 700 °C, gradual burn-off of surface carbon is evident. The carbon content based on the TGA is given in Table 1 and is in the range between 1.49 and 2.19 wt.%. Grouping of samples was based on the initially adsorbed drug—samples loaded with DS lost around 2.18 wt.% while samples used for IBU adsorption carried 1.49 and 1.73 wt.% of carbon, respectively. The higher mass loss observed for the DS-containing materials pointed to the formation of a more defect-rich and less thermally stable carbon phase, which is in agreement with the Raman spectra showing a stronger contribution of disorder-related carbon features.

Table 1. Calculated mass loss for samples based on TG analysis.

Sample	Water Mass Loss/wt.%	Carbon Mass Loss/wt.%
c-IBU@HB	1.50	1.49
c-IBU@OB	1.50	1.73
c-DS@HB	2.27	2.19
c-DS@OB	2.50	2.18

Samples derived from DS adsorption showed higher mass loss up to 300 °C, possibly due to less thermally stable aldehyde/ketone and carboxyl groups [47]. Another abrupt decrease in mass occurs between 500 and 700 °C, which is predominantly associated with thermal decomposition of carboxylic anhydride, phenol, and lactone groups [47], with again higher loss for the DS-loaded samples compared to the IBU-loaded samples, pointing to the resulting samples having more oxygen- and nitrogen-rich carbon surfaces when transformed with DS vs. IBU.

When looking at heat flow and temperature of degradation (Figure 3b), another distinction can be seen, as the samples with adsorbed IBU exhibit maximum burn-off around 638 °C, while those with DS burn at a higher temperature (661 °C), indicating more stable surface groups on DS-saturated organobentonites after carbonization [47]. The only stable groups remaining after temperature treatment should be carbonyl/quinone groups, known to be active in energy storage via a protonation/deprotonation mechanism [48].

3.4. Capacitance

The energy storage potential of the repurposed adsorbents after carbonization was probed in acidic (1 M H_2SO4), neutral (1 M Na_2SO_4), and alkaline (3 M KOH) media as shown in Figure 4a for sample c-IBU@OB. The CVs show a pronounced slant stemming from the high resistance of bentonite, which constitutes a high mass portion in the repurposed material (as evidenced by the TGA), a typical feature of electrically resistive materials [49]. Comparative cyclovoltammograms (CVs) in an alkaline environment showed current responses to a 10 mV/s sweeping potential (Figure 4b), with slight differences depending on the precursor composition. The obtained values for gravimetric capacitance are given in Table 2, with the highest values obtained for sample c-IBU@OB of around 20 F/g, in both acidic and basic conditions, when normalizing to the complete mass of the electrode, which can be explained by it having the highest content of surface carbon (around 34 wt.% based on EDX). However, using the TGA data, we can normalize the capacitance to just the carbon mass, under the assumption of negligible bentonite capacitance. Within this framework, significantly higher capacitance values are obtained, reaching exorbitant values of between 700 and 800 F/g in acidic and basic environments, similar to 710 F/g for quinone-decorated CNTs [50], 567 F/g for anthraquinone-2-sulfonate@rGO [51], DM-quinone decorated on reduced rGO with 650 F/g [52], and less than 1180 F/g for quinone–dopamine conjugates [53]. Based on the TGA, we suspect a quinone-covered carbon surface on the bentonite, which is corroborated by the maxima at −0.8 V (cathodic) and −0.45 V (anodic) in the alkaline, and 0.1 V [54] and 0.55 V (anodic and cathodic) in the acidic environment. Values in the neutral medium range between 300 and 400 F/g, with the literature relating the decreased capacitance to lower ionic conductivity and slower ion movement, compared to H^+ and OH^- in acidic and basic medium, respectively. Also, protonation/deprotonation peaks were absent in neutral media. Thermal regulation of carbon surface groups could therefore present a step towards high-capacitance materials.

Table 2. Capacitance (F g^{-1}) of carbonized organobentonites in studied electrolytes normalized to carbon content.

Sweep Rate/ mV s^{-1}	Base	Neut.	Acid	Base	Neut.	Acid	Base	Neut.	Acid	Base	Neut.	Acid
		c-IBU@OB			c-DS@OB			c-IBU@HB			c-DS@HB	
200	159 ± 6	64 ± 4	123 ± 6	116 ± 6	75 ± 5	138 ± 6	108 ± 4	56 ± 3	96 ± 5	82 ± 6	50 ± 3	97 ± 5
100	250 ± 8	92 ± 6	172 ± 8	155 ± 7	105 ± 6	186 ± 6	154 ± 4	79 ± 3	131 ± 5	112 ± 6	72 ± 6	129 ± 6
50	389 ± 8	136 ± 5	251 ± 9	207 ± 8	151 ± 6	265 ± 7	215 ± 5	118 ± 4	187 ± 6	152 ± 7	106 ± 6	184 ± 6
20	591 ± 9	226 ± 7	435 ± 10	282 ± 9	251 ± 8	457 ± 10	314 ± 5	201 ± 6	320 ± 7	210 ± 7	180 ± 8	292 ± 7
10	806 ± 12	372 ± 10	734 ± 12	363 ± 11	398 ± 9	806 ± 14	419 ± 6	332 ± 7	536 ± 9	268 ± 8	301 ± 10	485 ± 8

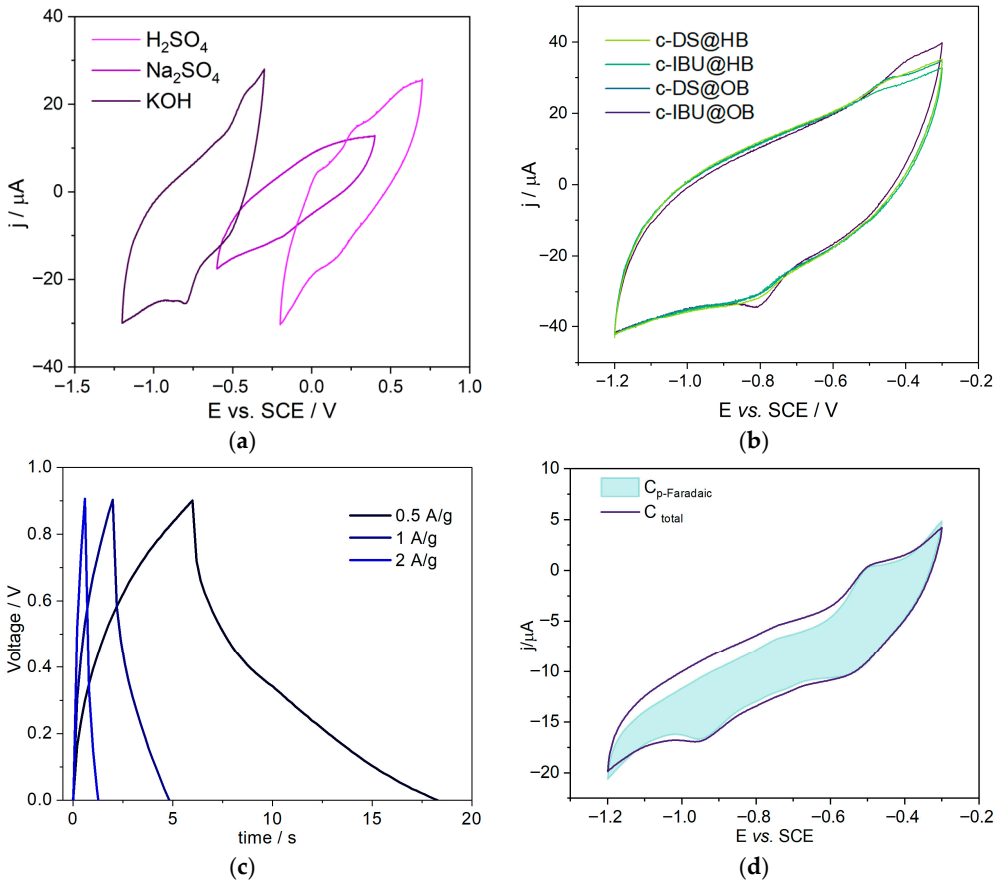


Figure 4. CV responses for (**a**) cIBU@OB in the studied electrolytes; (**b**) all samples in KOH; (**c**) charge/discharge curves for c-IBU@OB at different rates; and (**d**) pseudo-Faradaic contribution to overall capacitance according to Dunn analysis for c-IBU@OB.

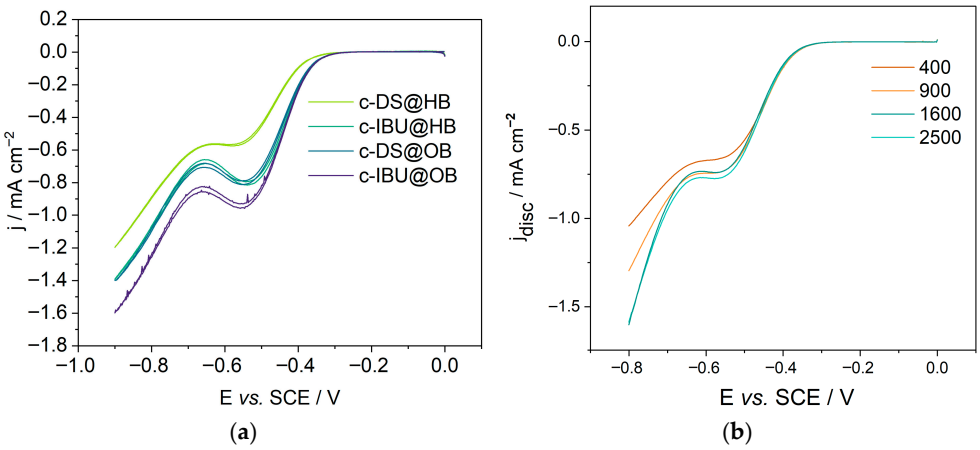
The gravimetric capacitance normalized to carbon content strongly depended on both the scan rate and electrolyte composition (Table 2). For all the samples, capacitance decreased with increasing sweep rate, reflecting diffusion limitations and reduced accessibility of electroactive sites at higher polarization rates. The highest capacitance values were consistently obtained in the KOH electrolyte, followed by H_2SO_4 and Na_2SO_4. At a sweep rate of 10 mV s^{-1}, the maximum capacitance reached 805.8 F g^{-1} in KOH, while substantially lower values were recorded in Na_2SO_4, indicating less efficient ion transport in the neutral electrolyte. The enhanced performance in KOH can be attributed to the high ionic conductivity and favorable mobility of hydroxide ions within the porous carbon structure, and pseudo-Faradaic reaction. Despite the decrease in capacitance with increasing scan rate, all the materials retained appreciable charge-storage capability at 200 mV s^{-1}, demonstrating good electrochemical accessibility of the carbon surface. Significant differences among the samples indicated that the chemical nature of the precursor plays an important role in determining the electrochemical properties of the resulting carbons. When considered together with the thermal and spectroscopic analyses, the capacitance data suggest that the adsorbed pharmaceutical influences the development of the carbon structure to a greater extent than the surfactant used for organobentonite preparation, leading to measurable differences in electrochemical performance. The particularly notable result is the 805.8 F g^{-1} capacitance in KOH, which is exceptionally high for a bentonite-derived carbon and suggests that, beyond double-layer charging, pseudocapacitive contributions from quinone surface groups must be present. Galvanostatic charge/discharge measurements were performed in a symmetric device at different charge/discharge rates (0.5, 1, 2 A g^{-1}), see Figure 4c, and capacitance was calculated based on Equation 3. When calculated as

the complete material mass, capacitance reached 6 F g^{-1} (@0.5 A g^{-1}), and 359 F g^{-1} when taking into account only the carbon-coating mass. These values are lower than those obtained under CV conditions, but this is expected as the results from two-electrode cell measurements are affected by internal resistance, electrode–electrolyte interfaces, and mass transport limitations within the entire cell structure [49,55]. A Dunn analysis [56,57], used for decoupling the electric double layer from the pseudo-Faradaic contribution (Figure 4d), showed that ≈83% of the capacitance stemmed from pseudo-Faradaic processes, i.e., protonation/deprotonation on quinone and other oxygen groups. The remaining 17% could be attributed to EDLC on the sp^2 carbon adlayer and, possibly, part of the uncovered bentonite.

3.5. Oxygen Reduction Catalysis

Baseline-corrected negative sweep scans of CVs in alkaline media at a rotation rate of 1600 were measured for all the samples and are shown in Figure 5a. All the samples exhibited comparable onset potentials for the ORR, while differences in the diffusion-limited current density indicated that both the surfactants used for bentonite modification and the adsorbed pharmaceuticals influenced the electrocatalytic performance of the resulting carbon. Among the investigated samples, carbon obtained from diclofenac sodium-loaded HDTMA-modified bentonite (c-DS@HB) showed the highest ORR activity, suggesting that the nitrogen content of the adsorbed drug prior to carbonization plays an important role in determining the structure and density of electrochemically active sites in the final carbon material. The activity of c-DS@HB may be attributed to nitrogen incorporated into the carbon framework during carbonization, as seen in EDX (around 6.6 at. %), as nitrogen-doped carbon materials are well known to exhibit enhanced ORR activity [34,58]. Therefore, sample c-DS@HB was selected for testing under different rates (400, 900, 1600, 2500 rpm), given in Figure 5b. The onset potential, of around −0.37 V, is slightly more negative in value than that of other carbon types and does not change upon cycling [59,60], indicating a stable structure of the active center for ORR. This negative shift could be attributed to the resistive nature of the adsorbent, which contributes significantly to the IR drop and subsequent negative shift in onset potential. An increase in plateau current (−0.5 to −0.7 V) with increasing rotation rates is direct proof that diffusion plays a role in the oxygen reduction [59]. The current plateaus are at a less negative current value than expected, and may be attributed to hindered oxygen reduction in the bentonite pores and hindered movement of reactant/products towards/away from the active sites inside the bentonite pores. Still, diffusion-limited current is established in this 200 mV-wide region, albeit at lower values than expected. Furthermore, the rise in current at even more negative potentials is still kinetically controlled due to low bentonite conductivity towards active sites on the carbon adlayer, and does not reach the diffusion-limiting current until the vertex condition of −0.9 V vs. SCE.

Oxygen reduction can proceed either toward a complete $4e^-$ reduction, desirable in fuel cells, or toward a $2e^-$ pathway in which peroxide is the main product. Modern electrochemical research promotes this route for peroxide formation as favorable to that of present-day commercial processes due to its lower cost, environmental friendliness, and scalability. To assess the oxygen reduction mechanism on our carbon-decorated bentonite, we used RRDE measurement, which showed almost exclusive formation of peroxide (Figure 6, Table 3).



(**a**) (**b**)

Figure 5. (**a**) CVs of carbonized NSAID-loaded organobentonites at 1600 rpm and (**b**) RDE polarization curves of c–DS@HB at different rotation rates in 0.1 M KOH.

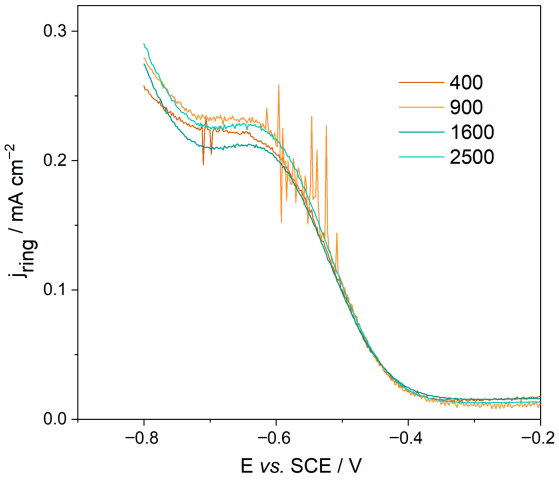


Figure 6. Ring–disk current densities of c–DS@HB electrode recorded at different rotation rates (400–2500 rpm) in 0.1 M KOH.

Table 3. Measured H_2O_2 yield at different rpm at the RRDE electrode with calculated n.

rpm@−0.6 V	H_2O_2 Yield/%	Apparent Number of Exchanged Electrons, n
300	92.7	2.15
900	88.7	2.23
1600	90.4	2.19
2400	87.6	2.24

The apparent number of exchanged electrons, n, is slightly above 2, suggesting a dominant 2e$^-$ pathway with some peroxide being reduced further. Looking at the peroxide yield, it can be seen that between 87.6% and 92.7% of the oxygen was converted to peroxide, while around 10% was further converted to OH^-. The high specific yield is comparable to that found in the literature for oxidized-CNT [61], hydrophobic vertical graphene [62], and a single-atom catalyst [63,64], all of which have significantly higher costs. We calculated the H_2O_2 production rate, based on our laboratory setup, to be 7.73 µmol h^{-1}, equivalent to 61.54 µmol cm^{-2} h^{-1} when normalized to the disk geometric area, or 15.46 mol g^{-1} h^{-1} when normalized to the catalyst mass, in line with recent literature data for carbon materials [65,66].

Carbon-decorated bentonite, produced by high-temperature carbonization after its initial use as an adsorbent for pollutant removal, represents a promising strategy for the valorization of abundant natural clay materials. Furthermore, tailoring the electroactive properties of carbonized organobentonites enables their performance to be optimized for specific applications, as the nature of the adsorbed pharmaceutical strongly influences the availability of electroactive sites and, consequently, their energy storage and peroxide production performance.

4. Conclusions

Successful conversion of bentonite loaded with ibuprofen or diclofenac sodium to a carbon-decorated adsorbent was performed with inert temperature carbonization. A TGA analysis showed 40 wt.% mass loss in an inert atmosphere and around a further 2 wt.% loss in air. Further mass loss in synthetic air points to the conclusion of there being a thin carbon layer on the bentonite after the initial temperature treatment in argon. The prepared materials have similar properties regarding electrochemical energy storage and activity towards ORR. FTIR and Raman spectroscopies confirmed defect-rich carbon on the adsorbent surface, while the TGA showed that after the treatment, only quinone groups survived. The same conclusion can be inferred from the CVs in alkaline and acidic environments, where maxima associated with this group can be seen. Capacitance values of 20 F/g are calculated when considering both the bentonite and carbon mass, while up to 805 F/g is calculated when normalizing only to carbon mass. Removing transformed carbon can therefore be a way towards obtaining a highly active material and regaining the adsorbent for reuse. The materials also possess high selectivity towards peroxide production in an alkaline environment (>92%), on par with high-cost alternatives, and could therefore be used for its production on site, which would be environmentally friendly and affordable. The presented results give an eco-friendly route from waste to highly selective materials in niche applications.

Author Contributions: Conceptualization, M.M.-R. and N.G.; methodology, M.O., M.R. and A.J.; software, B.N.V.; validation, H.W., A.D. and D.B.-B.; formal analysis, M.O., M.R., D.B.-B. and N.G.; investigation, B.N.V. and A.J.; data curation, M.O., M.R., D.B.-B. and N.G.; writing—original draft preparation, M.O., D.B.-B., M.M.-R. and N.G.; writing—review and editing, H.W., A.D., M.M.-R. and N.G.; visualization, N.G.; supervision, M.M.-R. All authors have read and agreed to the published version of the manuscript.

Funding: This research was funded by the Ministry of Science, Technological Development and Innovation of the Republic of Serbia (grant numbers 451-03-34/2026-03/200146, 451-03-33/2026-03/200146, 451-03-33/2026-03/200023, and AIRES project number 003417039), the National Key Research and Development Program (2024YFE0117300), National Natural Science Foundation of China (52575678), the interdisciplinary program of science and engineering from China University of Mining and Technology.

Institutional Review Board Statement: Not applicable.

Informed Consent Statement: Not applicable.

Data Availability Statement: The original data presented in the study are openly available in Zenodo repository at https://doi.org/10.5281/zenodo.21301295.

Conflicts of Interest: The authors declare no conflicts of interest.

References

1. aus der Beek, T.; Weber, F.-A.; Bergmann, A.; Hickmann, S.; Ebert, I.; Hein, A.; Küster, A. Pharmaceuticals in the Environment—Global Occurrences and Perspectives. *Environ. Toxicol. Chem.* **2015**, *35*, 823–835. [CrossRef]

2. Hussain, A.; Ashique, S.; Hassan, M.Z.; Afzal, O.; Asiri, Y.I.; Kumar, P.; Dua, K.; Webster, T.J.; Altamimi, A.S.A.; Altamimi, M.A. Pharmaceutical Contaminants in Aquatic Systems, Conventional and Green Strategies, Recent Updates, Challenges and Policies, and Potential Outcomes. *J. Mol. Liq.* **2023**, *389*, 122905. [CrossRef]
3. Arumugam, A.; Lee, K.E.; Ng, P.Y.; Shamsuddin, A.S.; Zulkifli, A.; Goh, T.L. Pharmaceuticals in Water: Fate, Health Risks, Treatment and Governance for Sustainable Management. *Water Air Soil Pollut.* **2026**, *237*, 828. [CrossRef]
4. Aziz, K.H.H.; Mustafa, F.S.; Karim, M.A.H.; Hama, S. Pharmaceutical Pollution in the Aquatic Environment: Advanced Oxidation Processes as Efficient Treatment Approaches: A Review. *Mater. Adv.* **2025**, *6*, 3433–3454. [CrossRef]
5. Madikizela, L.M.; Netshithothole, R. Non-Steroidal Anti-Inflammatory Drugs, Analgesics, and Their Metabolites in the Coastal Environment: The Escape to Seawater and Concerns. *Environ. Sci. Adv.* **2026**, *5*, 927–940. [CrossRef]
6. Gómez-Oliván, L.M. (Ed.) *Non-Steroidal Anti-Inflammatory Drugs in Water*; Springer International Publishing: Cham, Switzerland, 2020; Volume 96, ISBN 978-3030562939.
7. Murali, V. From Prescription to Pollution: The Ecological Consequences of NSAIDs in Aquatic Ecosystems. *Toxicol. Rep.* **2024**, *13*, 101775. [CrossRef]
8. Lin, J.; Zhang, Y.; Bian, Y.; Zhang, Y.; Du, R.; Li, M.; Tan, Y.; Feng, X. Non-Steroidal Anti-Inflammatory Drugs (NSAIDs) in the Environment: Recent Updates on the Occurrence, Fate, Hazards and Removal Technologies. *Sci. Total Environ.* **2023**, *904*, 166897. [CrossRef]
9. Patel, M.; Kumar, R.; Kishor, K.; Mlsna, T.; Pittman, C.U.; Mohan, D. Pharmaceuticals of Emerging Concern in Aquatic Systems: Chemistry, Occurrence, Effects, and Removal Methods. *Chem. Rev.* **2019**, *119*, 3510–3673. [CrossRef]
10. Mlunguza, N.Y.; Ncube, S.; Nokwethemba Mahlambi, P.; Chimuka, L.; Madikizela, L.M. Adsorbents and Removal Strategies of Non-Steroidal Anti-Inflammatory Drugs from Contaminated Water Bodies. *J. Environ. Chem. Eng.* **2019**, *7*, 103142. [CrossRef]
11. Ngernyen, Y.; Petsri, D.; Sribanthao, K.; Kongpennit, K.; Pinijnam, P.; Pedsakul, R.; Hunt, A.J. Adsorption of the Non-Steroidal Anti-Inflammatory Drug (Ibuprofen) onto Biochar and Magnetic Biochar Prepared from Chrysanthemum Waste of the Beverage Industry. *RSC Adv.* **2023**, *13*, 14712–14728. [CrossRef]
12. He, H.; Ma, Y.; Zhu, J.; Yuan, P.; Qing, Y. Organoclays Prepared from Montmorillonites with Different Cation Exchange Capacity and Surfactant Configuration. *Appl. Clay Sci.* **2010**, *48*, 67–72. [CrossRef]
13. Salihi, E.Ç.; Mahramanlıoğlu, M. Equilibrium and Kinetic Adsorption of Drugs on Bentonite: Presence of Surface Active Agents Effect. *Appl. Clay Sci.* **2014**, *101*, 381–389. [CrossRef]
14. Li, Y.; Jin, F.; Wang, C.; Chen, Y.; Wang, Q.; Zhang, W.; Wang, D. Modification of Bentonite with Cationic Surfactant for the Enhanced Retention of Bisphenol A from Landfill Leachate. *Environ. Sci. Pollut. Res.* **2015**, *22*, 8618–8628. [CrossRef]
15. He, H.; Xu, E.; Qiu, Z.; Wu, T.; Wang, S.; Lu, Y.; Chen, G. Phenol Adsorption Mechanism of Organically Modified Bentonite and Its Microstructural Changes. *Sustainability* **2022**, *14*, 1318. [CrossRef]
16. Arabmofrad, S.; Lazzara, G.; Miller, R.; Jafari, S.M. Surface Modification of Bentonite and Montmorillonite as Novel Nano-Adsorbents for the Removal of Phenols, Heavy Metals and Drug Residues. *Adv. Colloid Interface Sci.* **2024**, *334*, 103334. [CrossRef]
17. de Paiva, L.B.; Morales, A.R.; Valenzuela Díaz, F.R. Organoclays: Properties, Preparation and Applications. *Appl. Clay Sci.* **2008**, *42*, 8–24. [CrossRef]
18. Hacıosmanoğlu, G.G.; Mejías, C.; Martín, J.; Santos, J.L.; Aparicio, I.; Alonso, E. Antibiotic Adsorption by Natural and Modified Clay Minerals as Designer Adsorbents for Wastewater Treatment: A Comprehensive Review. *J. Environ. Manag.* **2022**, *317*, 115397. [CrossRef]
19. Anirudhan, T.; Ramachandran, M. Surfactant-Modified Bentonite as Adsorbent for the Removal of Humic Acid from Wastewaters. *Appl. Clay Sci.* **2007**, *35*, 276–281. [CrossRef]
20. Fraiha, O.; Hadoudi, N.; Zaki, N.; Salhi, A.; Amhamdi, H.; Akichouh, E.H.; Mourabit, F.; Ahari, M. Comprehensive Review on the Adsorption of Pharmaceutical Products from Wastewater by Clay Materials. *Desalin. Water Treat.* **2024**, *317*, 100114. [CrossRef]
21. Obradović, M.; Daković, A.; Smiljanić, D.; Ožegović, M.; Marković, M.; Rottinghaus, G.E.; Krstić, J. Ibuprofen and Diclofenac Sodium Adsorption onto Functionalized Minerals: Equilibrium, Kinetic and Thermodynamic Studies. *Microporous Mesoporous Mater.* **2022**, *335*, 111795. [CrossRef]
22. Obradović, M.; Daković, A.; Smiljanić, D.; Marković, M.; Ožegović, M.; Krstić, J.; Vuković, N.; Milojević-Rakić, M. Bentonite Modified with Surfactants—Efficient Adsorbents for the Removal of Non-Steroidal Anti-Inflammatory Drugs. *Processes* **2023**, *12*, 96. [CrossRef]
23. Obradović, M.; Daković, A.; Marković, M.; Smiljanić, D.; Ožegović, M.; Milojević-Rakić, M. Efficient Removal of Ibuprofen and Diclofenac Sodium Using Modified Bentonites: Adsorption Studies and Performance in Real Water. *Appl. Sci.* **2026**, *16*, 2585. [CrossRef]
24. Ghemit, R.; Makhloufi, A.; Djebri, N.; Flilissa, A.; Zerroual, L.; Boutahala, M. Adsorptive Removal of Diclofenac and Ibuprofen from Aqueous Solution by Organobentonites: Study in Single and Binary Systems. *Groundw. Sustain. Dev.* **2019**, *8*, 520–529. [CrossRef]

25. França, D.B.; Trigueiro, P.; Filho, E.C.S.; Fonseca, M.G.; Jaber, M. Monitoring Diclofenac Adsorption by Organophilic Alkylpyridinium Bentonites. *Chemosphere* **2020**, *242*, 125109. [CrossRef]
26. Smiljanić, D.; Obradović, M.; Marković, M.; Ožegović, M.; Daković, A.; Požega, E.; de Gennaro, B. Adsorption of Diclofenac and Ibuprofen on Organobentonites: Kinetic, Thermodynamic, and Simultaneous Adsorption. *J. Ind. Eng. Chem.* **2026**, *160*, 625–641. [CrossRef]
27. Panda, B. Waste-Derived Adsorbents for the Removal of Pollutants. In *Conversion and Utilization of Wastes into Sustainable Products*; Wiley: New York, NY, USA, 2026; pp. 375–409.
28. Rangappa, H.S.; Herath, I.; Lin, C.; Ch, S. Industrial Waste-Based Adsorbents as a New Trend for Removal of Water-Borne Emerging Contaminants. *Environ. Pollut.* **2024**, *343*, 123140. [CrossRef]
29. Fouda-Mbanga, B.G.; Onotu, O.; Tywabi-Ngeva, Z. Advantages of the Reuse of Spent Adsorbents and Potential Applications in Environmental Remediation: A Review. *Green Anal. Chem.* **2024**, *11*, 100156. [CrossRef]
30. Gkika, D.A.; Kyzas, G.Z. Reusability of Spent Adsorbents for a Circular Materials Economy in the Sustainable Chemical Industry. *RSC Sustain.* **2026**, *4*, 1023–1048. [CrossRef]
31. Gkika, D.A.; Tolkou, A.K.; Katsoyiannis, I.A.; Kyzas, G.Z. The Adsorption-Desorption-Regeneration Pathway to a Circular Economy: The Role of Waste-Derived Adsorbents on Chromium Removal. *Sep. Purif. Technol.* **2025**, *368*, 132996. [CrossRef]
32. Jevremović, A.; Ranković, M.; Ležajić, A.J.; Uskoković-Marković, S.; Vasiljević, B.N.; Gavrilov, N.; Bajuk-Bogdanović, D.; Milojević-Rakić, M. Regeneration or Repurposing of Spent Pollutant Adsorbents in Energy-Related Applications: A Sustainable Choice? *Sustain. Chem.* **2025**, *6*, 28. [CrossRef]
33. Popadić, D.; Krstić, J.; Ležaić, A.J.; Popović, M.; Milojević-Rakić, M.; Ignjatović, L.; Bajuk-Bogdanović, D.; Gavrilov, N. Acetamiprid's Degradation Products and Mechanism: Part II—Inert Atmosphere and Charge Storage. *Spectrochim. Acta A Mol. Biomol. Spectrosc.* **2024**, *308*, 123772. [CrossRef]
34. Popadić, D.; Gavrilov, N.; Ignjatović, L.; Krajišnik, D.; Mentus, S.; Milojević-Rakić, M.; Bajuk-Bogdanović, D. How to Obtain Maximum Environmental Applicability from Natural Silicates. *Catalysts* **2022**, *12*, 519. [CrossRef]
35. Zallouz, S.; Aumond, T.; Moissette, A.; Sachse, A.; Ghimbeu, C.M. Zeolite-Templated Carbons as Supercapacitors: The Fundamental Role of Structural and Textural Properties. *ACS Appl. Energy Mater.* **2024**, *7*, 9142–9155. [CrossRef]
36. Zhao, Z.; Zhang, Y.; Xiao, Y.; Wang, J.; Wang, T.; Pan, W.-P. Multilevel Regulation of Zeolite-Template Carbon: From Microscopic Physical Structure Optimization to Atomic Doping Synergistic Effect to Enhance Supercapacitor Performance. *J. Power Sources* **2026**, *664*, 238939. [CrossRef]
37. Khan, S.; Park, H.; Kim, K.; Park, H.; Ryoo, R. Hierarchically Porous Zeolite-Templated Carbon Embedded with Manganese Oxide for Long-Cycling Asymmetric Supercapacitor. *Microporous Mesoporous Mater.* **2024**, *369*, 113050. [CrossRef]
38. Ma, R.; Lin, G.; Zhou, Y.; Liu, Q.; Zhang, T.; Shan, G.; Yang, M.; Wang, J. A Review of Oxygen Reduction Mechanisms for Metal-Free Carbon-Based Electrocatalysts. *npj Comput. Mater.* **2019**, *5*, 78. [CrossRef]
39. Sun, B.; Zhang, M.; Zhou, N.; Chu, X.; Yuan, P.; Chi, C.; Wu, F.; Shen, J. Study on Montmorillonite–Chlorhexidine Acetate–Terbinafine Hydrochloride Intercalation Composites as Drug Release Systems. *RSC Adv.* **2018**, *8*, 21369–21377. [CrossRef]
40. Li, J.; Li, Z.; Zhang, R.; Zhao, L.; Niu, Q.; Dong, Y.; Li, J.; Fang, Z.; Lu, Q.; Li, K. Upcycling Spent Bleaching Clay into Clay/Carbon Composites for Adsorptive Removal of Pb(II). *Mater. Chem. Phys.* **2025**, *345*, 131306. [CrossRef]
41. Merikhy, A.; Heydari, A.; Eskandari, H.; Ghahraman-Rozegar, F. Carbonized Spent Bleaching Earth as a Low-Cost Adsorbent: A Facile Revalorization Strategy via Response Surface Methodology. *Chem. Eng. Process.-Process Intensif.* **2020**, *158*, 108167. [CrossRef]
42. Tang, J.; Mu, B.; Zong, L.; Zheng, M.; Wang, A. Fabrication of Attapulgite/Carbon Composites from Spent Bleaching Earth for the Efficient Adsorption of Methylene Blue. *RSC Adv.* **2015**, *5*, 38443–38451. [CrossRef]
43. Zaitan, H.; Bianchi, D.; Achak, O.; Chafik, T. A Comparative Study of the Adsorption and Desorption of O-Xylene onto Bentonite Clay and Alumina. *J. Hazard. Mater.* **2008**, *153*, 852–859. [CrossRef]
44. Schwan, J.; Ulrich, S.; Batori, V.; Ehrhardt, H.; Silva, S.R.P. Raman Spectroscopy on Amorphous Carbon Films. *J. Appl. Phys.* **1996**, *80*, 440–447. [CrossRef]
45. Zyoud, A.H.; Zyoud, S.H.; Amireh, A. An Innovative and Sustainable Approach for Water Purification: Thermal Decomposition of Tetracycline Contaminant Adsorbed on Thermally Stable Montmorillonite. *Case Stud. Chem. Environ. Eng.* **2024**, *9*, 100631. [CrossRef]
46. Dittmann, D.; Eisentraut, P.; Goedecke, C.; Wiesner, Y.; Jekel, M.; Ruhl, A.S.; Braun, U. Specific Adsorption Sites and Conditions Derived by Thermal Decomposition of Activated Carbons and Adsorbed Carbamazepine. *Sci. Rep.* **2020**, *10*, 6695. [CrossRef]
47. Jovanovic, Z.; Bajuk-Bogdanović, D.; Jovanović, S.; Mravik, Ž.; Kovač, J.; Holclajtner-Antunović, I.; Vujković, M. The Role of Surface Chemistry in the Charge Storage Properties of Graphene Oxide. *Electrochim. Acta* **2017**, *258*, 1228–1243. [CrossRef]
48. Ega, S.P.; Srinivasan, P. Quinone Materials for Supercapacitor: Current Status, Approaches, and Future Directions. *J. Energy Storage* **2022**, *47*, 103700. [CrossRef]

49. Azizpour, A.; Bagovic, N.; Ploumis, N.; Mylonas, K.; Hoxha, D.; Kienberger, F.; Al-Zubaidi-R-Smith, N.; Gramse, G. Electrochemical Analysis of Carbon-Based Supercapacitors Using Finite Element Modeling and Impedance Spectroscopy. *Energies* **2025**, *18*, 1450. [CrossRef]
50. Chen, X.; Wang, H.; Yi, H.; Wang, X.; Yan, X.; Guo, Z. Anthraquinone on Porous Carbon Nanotubes with Improved Supercapacitor Performance. *J. Phys. Chem. C* **2014**, *118*, 8262–8270. [CrossRef]
51. Shi, R.; Han, C.; Duan, H.; Xu, L.; Zhou, D.; Li, H.; Li, J.; Kang, F.; Li, B.; Wang, G. Redox-Active Organic Sodium Anthraquinone-2-Sulfonate (AQS) Anchored on Reduced Graphene Oxide for High-Performance Supercapacitors. *Adv. Energy Mater.* **2018**, *8*, 1802088. [CrossRef]
52. Boota, M.; Chen, C.; Bécuwe, M.; Miao, L.; Gogotsi, Y. Pseudocapacitance and Excellent Cyclability of 2,5-Dimethoxy-1,4-Benzoquinone on Graphene. *Energy Environ. Sci.* **2016**, *9*, 2586–2594. [CrossRef]
53. Ega, S.P.; Biradar, M.R.; Srinivasan, P.; Bhosale, S.V. Designing Quinone-Dopamine-Based Conjugates as Six Electron System for High-Performance Hybrid Electrode. *Electrochim. Acta* **2020**, *357*, 136835. [CrossRef]
54. Gao, X.; Du, D.; Li, S.; Yan, X.; Xing, W.; Bai, P.; Xue, Q.; Yan, Z. Outstanding Capacitive Performance of Ordered Mesoporous Carbon Modified by Anthraquinone. *Electrochim. Acta* **2018**, *259*, 110–121. [CrossRef]
55. Stoller, M.D.; Ruoff, R.S. Best Practice Methods for Determining an Electrode Material's Performance for Ultracapacitors. *Energy Environ. Sci.* **2010**, *3*, 1294. [CrossRef]
56. Harish, S.; Sathyakam, P.U. Dunn's Method for Distinguishing Charge Storage Mechanisms in Supercapacitors: A Status Quo Review. *J. Electron. Mater.* **2025**, *54*, 10858–10872. [CrossRef]
57. Matos-Peralta, Y.; Panaritis, C.; Hagler, J.; Santato, C.; Patience, G.S. Experimental Methods in Chemical Engineering: Cyclic Voltammetry—CV. *Can. J. Chem. Eng.* **2026**, *Epub ahead of printing*. [CrossRef]
58. Gavrilov, N.; Pašti, I.A.; Mitrić, M.; Travas-Sejdić, J.; Ćirić-Marjanović, G.; Mentus, S.V. Electrocatalysis of Oxygen Reduction Reaction on Polyaniline-Derived Nitrogen-Doped Carbon Nanoparticle Surfaces in Alkaline Media. *J. Power Sources* **2012**, *220*, 306–316. [CrossRef]
59. Muñoz-Morales, M.; Ramírez, A.; Cañizares, A.; Llanos, J.; Ania, C. Evaluating Key Properties of Carbon Materials as Cathodes for the Electrogeneration of Hydrogen Peroxide. *Carbon* **2023**, *210*, 118082. [CrossRef]
60. Zhao, X.; Zou, X.; Yan, X.; Brown, C.L.; Chen, Z.; Zhu, G.; Yao, X. Defect-Driven Oxygen Reduction Reaction (ORR) of Carbon without Any Element Doping. *Inorg. Chem. Front.* **2016**, *3*, 417–421. [CrossRef]
61. Liu, W.; Li, C.; Ding, G.; Duan, G.; Jiang, Y.; Lu, Y. Highly Efficient Hydrogen Peroxide Electrosynthesis on Oxidized Carbon Nanotubes by Thermally Activated-Persulfate. *J. Mater.* **2022**, *8*, 136–143. [CrossRef]
62. Zhang, D.; Tsounis, C.; Peng, L.; Yin, H.; Hussain, F.; Carnell, M.; Macmillan, A.; Chu, D.; Amal, R.; Han, Z. Nitrogen-Doped Vertical Graphene for Highly Efficient Hydrogen Peroxide Electrosynthesis in Acidic Environment. *Chem. Eng. J.* **2024**, *496*, 154221. [CrossRef]
63. Wang, Z.; Jia, H.; Xie, A.; Li, Y.; Chen, Z.; Lu, X.; Zhao, H. Structure-Adaptive Single-Atom Nickel Catalysts for Pure Hydrogen Peroxide Electrosynthesis at Industrial Current Density. *Nat. Commun.* **2026**, *17*, 4431. [CrossRef]
64. Chen, K.-Y.; Huang, Y.-X.; Jin, R.-C.; Huang, B.-C. Single Atom Catalysts for Use in the Selective Production of Hydrogen Peroxide via Two-Electron Oxygen Reduction Reaction: Mechanism, Activity, and Structure Optimization. *Appl. Catal. B* **2023**, *337*, 122987. [CrossRef]
65. Mavrikis, S.; Couce, P.M.; Göltz, M.; Feith, D.W.; Waddy, N.N.H.; Bisselink, R.J.M.; van Haasterecht, T.; Schweiß, R.; Rosiwal, S.; de León, C.P.; et al. Practical Electrochemical Production of Hydrogen Peroxide via Paired Two-Electron Oxygen Reduction and Water Oxidation. *Chem. Eng. J.* **2026**, *542*, 177643. [CrossRef]
66. Liu, J.; Zhang, Z.; Xu, Z.; Zhu, Y.; Han, C.; Xiong, W.; Attfield, J.P.; Zeng, J.; Liu, S.; Yang, M. Tailoring Oxygen Adsorption on Nickel Nitride for Selective 2e− ORR to Hydrogen Peroxide. *Chem. Eng. J.* **2025**, *519*, 165448. [CrossRef]

Disclaimer/Publisher's Note: The statements, opinions and data contained in all publications are solely those of the individual author(s) and contributor(s) and not of MDPI and/or the editor(s). MDPI and/or the editor(s) disclaim responsibility for any injury to people or property resulting from any ideas, methods, instructions or products referred to in the content.